JAIST Repository
https://dspace.jaist.ac.jp/

Title	Low Temperature Heteroepitaxial Growth of a New Phase Lead Zirconate Titanate Film on Si Substrate with an Epitaxial (Zr0_2)_<1-x>(Y_20_3)_x Buffer Layer
Author(s)	Horita, Susumu; Aikawa, Mami; Naruse, Tetsuya
Citation	Japanese Journal of Applied Physics, 39: 4860-4868
Issue Date	2000
Type	Journal Article
Text version	author
URL	http://hdl.handle.net/10119/9600
Rights	This is the author's version of the work. It is posted here by permission of The Japan Society of Applied Physics. Copyright (C) 2000 The Japan Society of Applied Physics.
Description	

JAIST
JAPAN ADVANCED INSTITUTE OF SCIENCE AND TECHNOLOGY

Japan Advanced Institute of Science and Technology

Low Temperature Heteroepitaxial Growth of a New Phase Lead Zirconate Titanate Film on Si Substrate with an Epitaxial $(ZrO_2)_{1-x}(Y_2O_3)_x$ Buffer Layer

Susumu HORITA*, Mami AIKAWA and Tetsuya NARUSE

School of Materials Science, Japan Advanced Institute of Science and Technology, Hokuriku, Tatsunokuchi, Ishikawa 923-1292, Japan

(Received date; revised manuscript received date; accepted for publication date — These dates will be written in by the editor, hence please let these lines remain unchanged even though your preprint looks a bit ugly.)

We investigated the crystalline and electrical properties of heteroepitaxial lead zirconate titanate (PZT) films grown on Si covered with epitaxial (100) $(ZrO_2)_{1-x}(Y_2O_3)_x$(YSZ) buffer layers. The PZT films were prepared by reactive sputtering. When the substrate temperature was between 400 and 485°C, we obtained a heteroepitaxial (110) oriented monoclinic PZT (m-PZT) film which was metastable. The lattice parameters were as follows: $a = b = 0.379$ nm, $c = 0.521$ nm and $\gamma = 81.3°$. The m-PZT film had a larger oxygen composition ratio O/(Zr+Ti) of 3.2 to 3.8 than the perovskite phase. Although the resistivity of the as-grown m-PZT film was much lower than that of the normal perovskite phase, it was increased by two to five orders of magnitude by a step-annealing process of 300°C for 120 min, 325°C for 120 min and 350°C for 180 min in sequence. From the $C-V$ characteristics of the step-annealed m-PZT/YSZ/Si structure, the relative dielectric constant was estimated to be about 45.

KEYWORDS: PZT, YSZ, Si, heteroepitaxy, sputtering, monoclinic

1. Introduction

Lead zirconate titanate $Pb(Zr_xTi_{1-x})O_3$(PZT) has recently been studied as a promising material for capacitors in ferroelectric random-access memories (FRAMs) and for gate dielectric insulators in metal/ferroelectric/semiconductor field-effect transistors (MFS- FETs).[1,2] MFS-FETs, in which the gate is controlled by spontaneous polarization of ferroelectric materials, have the features of high switching speed, nonvolatility, radiation tolerance and high density. To realize MFS-FETs, it is necessary to fabricate PZT films directly on semiconductor substrates, in particular, on Si. However, this is very difficult because Pb reacts with Si and easily diffuses into the Si substrate.[3] In order to overcome this difficulty, several researchers attempted to use several dielectric materials, *e.g.*, CeO_2,[2] MgO,[4,5] $SrTiO_3$,[6] $Ce_xZr_{1-x}O_2$,[7] Y_2O_3[8] and ZrO_2[9] as a buffer layer inserted between the PZT film and the Si substrate. On the other hand, a single crystal film is expected to exhibit high stability, uniformity of material properties and high performance of electron device.[10,11] In order to obtain an epitaxial single crystal PZT film, the buffer layer should be a single crystal film. Thus, we have proposed the use of a heteroepitaxial yttria- stabilized zirconia [YSZ;$(ZrO_2)_{1-x}(Y_2O_3)_x$] film as a buffer layer.[12,13] YSZ is a very attractive electrical insulator because it has high chemical stability, high resistivity and a large relative dielectric constant of about 30, and can be heteroepitaxially grown on Si.[14] Hirai *et al.* used a YSZ layer as a buffer layer for $PbTiO_3$ on Si.[15] Also, we have reported that an epitaxial PZT film on Si can be obtained with a 10-nm-thick epitaxial YSZ layer.[12] In order to operate MFIS-FET at a lower voltage in future ICs, it is necessary to make the YSZ buffer layer as thin as possible. However, because decreasing the thickness of the YSZ buffer layer leads to a reduction in its ability to prevent the diffusion of Pb into the Si substrate, the growth temperature of the PZT film has to be lowered. Also, the low temperature growth technique has the advantage of controlling the Pb content of the film more easily than the high temperature growth because it suppresses the re-evaporation of Pb and Pb oxides from the deposition surface.[16,17] Thus, we attempted the low temperature deposition of PZT film on an epitaxial YSZ layer by rf magnetron sputtering and obtained an epitaxial PZT film at substrate temperatures as low as 435°C. However, this epitaxial PZT film showed material properties different from those of a perovskite PZT film. In order to improve electrical insulation, we annealed the deposited PZT films. In this paper, we report the crystalline properties, electrical properties and chemical composition of as-grown and annealed PZT films, and discuss the experimental results.

2. Experimental

YSZ buffer layers were deposited on n-type (100) Si substrates by dc magnetron reactive sputtering with $Ar+O_2$ gas and a metallic target. The resistivity of the substrate was 0.005-0.01 Ωcm. Generally, the heteroepi-

*E-mail address: horita@jaist.ac.jp

taxial growth of a YSZ layer on Si by reactive sputtering is difficult because the bare Si surface is easily oxidized by plasma radiation or excited oxygen atoms prior to the deposition of the YSZ layer. As a solution to this problem, we used the following process: the Si surface is weakly oxidized, followed by deposition of a very thin metallic $Zr_{1-m}Y_m$ film prior to the deposition of a YSZ layer. The details of this process are shown elsewhere.[18] The thickness of the YSZ layer was about 10 or 100 nm and the yttria content was estimated to be about 14 mol% by X-ray photoelectron spectroscopy (XPS) measurement with a standard sample. The PZT film was deposited on the YSZ/Si structure by rf magnetron reactive sputtering. We used a 4-inch-diameter stoichiometric $Pb(Zr_{0.52}Ti_{0.48})O_3$ disc as a sputtering target. Since the substrate temperature was relatively low, 435-520°C, it was expected that the re-evaporation of Pb and PbO from the deposition surface was suppressed so that the composition of the deposited film became nearly equal to that of the target.[19] The substrate was heated by flowing electric current through the tantalum electrodes attached to the substrate. The typical sputtering conditions were as follows: the discharge pressure of $Ar+O_2$ gas was 2 Pa, the O_2/Ar flow rate ratio was 1/10 and the rf power was 100 W. The thickness of the PZT film was 100 or 200 nm. In order to improve the electrical properties of the as-grown PZT films, some of them were annealed at a temperature of 300 to 400°C in O_2 atmosphere.

The crystallographic properties of the PZT films were investigated by X-ray diffraction (XRD) analysis and Rutherford backscattering (RBS) spectrometry with 1.6 MeV $^4He^+$ ions. The chemical composition of the sample was also obtained by RBS measurement. Microstructural characterization of the samples was carried out using a transmission electron microscope (TEM). Leakage current density-voltage ($J-V$) characteristics were measured with step voltages and the time interval of each step was 2 s. Top and bottom electrodes were formed by depositing 0.2-mm-diameter Au and Al films on the PZT film and on the back of the substrate, respectively.

3. Experimental Results

Figure 1 shows the substrate temperature T_S dependence of XRD patterns of 100- or 200-nm-thick PZT films on Si with YSZ buffer layers. The thicknesses of the YSZ layers are 10 nm at $T_S = 460$ and 470°C, and 100 nm at $T_S = 435$ and 495°C. The peaks due to YSZ (200) are hardly observed at $T_S = 460$ and 470°C because they overlap with the large pyrochlore (400) peaks. We can see from this figure that strong peaks near the diffraction angle of the perovskite PZT (110) around 31° appear with small peaks around 34.3° due to pyrochlore (400) and 36.2°, when T_S is equal or less than 470°C. The peaks around 36.2° are not due to YSZ, PZT and PbO. On the other hand, at the higher substrate temperature $T_S \geq 495$°C, the diffraction peak due to the pyrochlore (400) phase becomes strong and the peak around 31° disappears. The peak angle of this pyrochlore phase is slightly smaller than those at $T_S = 460$ and 470°C. This

Fig. 1

phenomenon probably results from the influence of the underlying YSZ layer and is discussed further based on the results in Fig.6. Figure 2 shows the ϕ scan patterns of the PZT film grown at T_S = 435°C in Fig.1. From each pattern, we can observe peaks of four fold symmetry clearly. These patterns are very similar to those of the perovskite (110) PZT film with a heteroepitaxial double domain structure. A similar crystallographic orientation relation on heteroepitaxial growth has been reported for $(110)Y_2O_3/(100)Si$[20] and $(110)CeO_2/(100)Si$.[21] However, it was found that the values of θ for the measured lattice planes were different from those of the perovskite PZT. This difference can not be explained by measurement error and simple lattice deformation due to heteroepitaxial growth. This essentially results from the formation of an unknown PZT phase, which is explained more clearly by means of cross-sectional TEM observation as shown in Fig.6. Hereafter, this unknown PZT phase is abbreviated to m-PZT and its structure will be discussed in greater detail later.

Fig. 2

Next, we estimated the chemical composition of the deposited PZT film by RBS measurement. Figure 3 shows the dependence of the composition ratio of the deposited PZT film on the substrate temperature. The measurement error is about ±5%. The substrate temperatures are divided into the three regions with respect to the crystallinity of the deposited PZT film. The temperature of the first (I) region is between room temperature and 400°C, where the film is almost amorphous because of the absence of XRD peaks except those of Si and YSZ. The temperatures of the second (II) and third (III) regions are between 400 and 480°C, and higher than 480°C, respectively. In the II and III regions, the PZT films consist of mainly unknown and pyrochlore phases, respectively. From this figure, it can be seen that the Pb ratios range from 0.9 to 1.0 and are almost stoichiometric for all three temperature regions. Also, the Ti and Zr ratios are roughly constant over the substrate temperature range investigated, although they approach target values with a gradual increase in substrate temperature. Some researchers have reported the same results regarding the Ti and Zr composition ratios of PZT films prepared by sputtering.[22,23] In contrast, the oxygen composition ratio shows marked variation with substrate temperature: It is much higher in the II region than in the other temperature regions. Also, in the III region, it is smaller than the stoichiometric ratio of the perovskite phase, which means that the deposited film contains oxygen-deficient pyrochlore phase.

Fig. 3

In order to improve the electrical insulation of the m-PZT film, we annealed the as-grown samples. When the annealing temperature and time were set at 350°C and 90 min, respectively, the (110) m-PZT peak in the XRD pattern decreased in intensity and the crystalline quality of the m-PZT film deteriorated. Although the sample annealed at 300°C for 30 min retained the m-PZT phase, electrical insulation was not sufficiently improved. Then, the sample annealed at 300°C for 30 min was annealed again at 400°C for 30 min. However, the crystalline quality of the m-PZT film degraded, accompanied by the formation of a small amount of pyrochlore phase, as

shown in Fig.4(a), where the m-PZT film was grown at T_S = 435°C. From these results, we consider that the m-PZT phase is metastable and more unstable than the pyrochlore phase. In order to avoid the phase change of the m-PZT film due to high temperature annealing, we attempted to use a step-annealing process which involves the three annealing conditions of 300°C for 120 min, 325°C for 120 min and 350°C for 180 min in sequence. Figure 4(b) shows the XRD pattern of the step-annealed sample with the PZT film grown at T_S = 460°C. From this figure, it can be seen that the XRD pattern of the step-annealed sample did not vary markedly from that of the as-grown one except for the small increase in intensity of the pyrochlore (400) peak. Figures 5(a) and 5(b) show the RBS spectra of the as-grown sample (Fig.1, T_S = 460°C) and the step-annealed sample (Fig.4 (b)), respectively. From these figures, it can be seen that the channeling minimum yields, χ_{min}, in the Pb band near the surface are about 60 and 90% for the as-grown and the step-annealed samples, respectively. The increase in χ_{min} due to the step-annealing process is likewise observed in the Ti and Zr bands of the PZT film. This means that the crystalline quality of the PZT film was deteriorated slightly by the step-annealing process, in agreement with the XRD measurement result of Fig.4. However, the inter-diffusion between the PZT film and the YSZ layer and the composition change due to the step-annealing process are hardly observed in the random RBS spectra. Since the step-annealing process with the temperature higher than 350°C might induce phase change, it was not performed.

Fig. 4

Fig. 5

Figure 6 shows the cross-sectional TEM images and the selected-area diffraction (SAD) patterns of the deposited PZT film, where the sample is the step-annealed one in Fig.4(b). The upper direction is toward the surface of the PZT film. From Figs.6(a) and 6(b), we observe three kinds of lattice images such as rectangular in region (1) of Fig.6(a), rhombus in region (3) of Fig.6(b) and square in region (4) of Fig.6(b). These lattice images correspond to the SAD patterns, *i.e.*, (1) of Fig.6(a) to Fig.6(c), (3) of Fig.6(b) to Fig.6(d), and (4) of Fig.6(b) to Fig.6(e). It can be recognized that the TEM image of (4) in Fig.6(b) and the SAD pattern in Fig.6(e) are obtained from the (100) pyrochlore PZT region in the film, judging from the lattice constant and crystallographic symmetry. The SAD patterns in Figs.6(c) and 6(d) are apparently different from those of the perovskite PZT phase; therefore, they are from the m-PZT phase. The details are discussed later. Also, area (2) in Fig.6(a) seems to be the phase transition region from m-PZT to pyrochlore. In the SAD patterns, particularly Fig.6(c), some spots are almost faint and some extra spots appear. This is probably because the uniform crystalline area is relatively small and comparable to the electron beam size of 3 nm so that the observed crystalline area contains small regions of different crystal structures. Another possible reason is that heating or bombardment to the film by the electron beam induces the phase transition from metastable m-PZT to pyrochlore. In fact, the TEM image was gradually changed as the electron beam current was increased during observation.

Fig. 6

On the other hand, the cross-sectional TEM image also shows that most of an about 20-nm-thick interfacial layer from the YSZ layer is pyrochlore phase. If this pyrochlore layer grew from the YSZ film, the phase of the growing film would not change from pyrochlore to m-PZT and all of the film would have the pyrochlore phase. This is because the pyrochlore phase is stabler than the m-PZT phase as mentioned above. Thus, it can be considered that this pyrochlore interfacial layer was formed due to the phase transition of the m-PZT phase film. It is also supposed that this transition occurred not during the step-annealing process but during the deposition or the cooling process after the deposition since the region comprising this layer is as large as about 1/5 of the entire PZT film and the pyrochlore peak intensity in the XRD pattern was not so increased by the step-annealing process as shown in Fig.4(b). As a candidate force that induces the phase transition, we have film stress due to the differences in the lattice constant and the thermal expansion coefficient between YSZ and PZT. Based on this consideration, we can explain the small difference in pyrochlore peak angle between the XRD patterns obtained at 495°C and 460 or 470°C, as shown in Fig.1, as follows: It can be deduced from the above discussion that the pyrochlore peaks at 460 and 470°C are mainly due to the pyrochlore interfacial layer. This thin interfacial layer is so strongly influenced by the YSZ layer that it may be slightly deformed. However, since the PZT film grown at 495°C is entirely pyrochlore with a thickness of 200 nm, the deformed structure in the interface is negligible compared with the entire average crystal structure. Therefore, the XRD peak angle due to the pyrochlore phase at 495°C is slightly different from those at 460 and 470°C.

Figure 7 shows the leakage current characteristics of the as-grown sample with a 10-nm-thick YSZ buffer layer at $T_S = 460°C$ and the step- annealed sample shown in Fig.4(b). We can see that the leakage current of the as-grown sample is much higher than that of a normal perovskite film. This leakage current was as high as that of the as-grown m-PZT film even with a 100-nm-thick YSZ buffer layer. Also, the leakage current of a 10-nm-thick YSZ/Si structure was lower than 10^{-7} A/cm^2 at 0.5 V. These results suggest that the resistivity of the as-grown m-PZT film should be sufficiently low that the leakage current of the as-grown film flows not through the YSZ layer but parallel to the surface of the m-PZT film to its edges which are in contact with the bare Si surface without the YSZ layer. However, the leakage current was markedly reduced by the step-annealing process by two to five orders of magnitude as shown in Fig.7. When the applied voltage is lower than 3 V, the leakage current of the step-annealed sample is lower than 1×10^{-7}A/cm^2. We can conclude from this result that the step-annealing process is very useful for improving the electrical insulation of the m-PZT film.

Fig. 7

In order to investigate the high electric conduction mechanism of the as- grown m-PZT film, we measured the temperature T dependence of electrical current I (A) at 3 V of the m-PZT film grown at $T_S = 460°C$ as shown in Fig.8, where the data are plotted as $\log(I)$ versus T

(closed circles) and $1/T$ (open circles). In this case, measurement was performed between the two top electrodes with 0.5 mm diameter and the distance from the center between them was about 2.3 mm. The current-voltage characteristics showed perfect ohmic behavior between 0 to 5 V. Therefore, Fig.8 indicates only film characteristics without the effect of the interface contact. It is clear that the current does not obey the Arrhenius law; rather, $\log(I)$-T is a good description of the data. A similar temperature dependence of current has been reported for the conductivity of Fe_3O_4 and this phenomenon can be explained by the incoherent tunneling of electrons between neighboring sites.[24,25)

Fig. 8

Figure 9 shows the $C-V$ characteristics of the 10-nm-thick YSZ/Si structure where the sweep rate is 0.1 V/s. The relative dielectric constant of the YSZ layer is estimated to be about 6 from the accumulation region capacitance of 530 nF/cm^2 and is much smaller than the bulk value. This means that a silicon oxide SiO_x transition layer was formed between the YSZ layer and the silicon substrate because the accumulation region capacitance is a series combination of YSZ layer and transition layer capacitances. This transition layer was formed by the diffusion of oxygen from the YSZ layer surface to the interface during YSZ layer deposition.[26) We can see from Fig.9 that the $C-V$ characteristics have a little hysteresis with a counterclockwise trace as indicated by the arrows probably because of the drift of mobile ions in the YSZ layer. We have reported that the hysteresis can be reduced by avoiding plasma radiation to the substrate during YSZ layer deposition.[27) Then, this hysteresis phenomenon is not an essential problem affecting the properties of the interface between the YSZ layer and the Si substrate and may be suppressed by optimizing the deposition conditions of the YSZ layer. Also, a kink behavior is observed around 1 V. One of the causes of this phenomenon is considered to be the high density of the interface near the conduction band edge of the Si due to crystalline defects. However, we are still investigating the origin of this kink behavior and will describe the details of the mechanism and the suppression method elsewhere. Although the $C-V$ characteristics of the YSZ/Si structure show slight hysteresis and the kink behavior near the flat-band state, they can be ignored from the viewpoint of the fundamental investigation of the $C-V$ characteristics of the m-PZT film deposited on the YSZ/Si structure.

Fig. 9

Figure 10 shows the $C-V$ characteristics of the step-annealed sample shown in Fig.4(b), where the sweep rates are 0.1, 0.5 and 1.0 V/s and the YSZ layer thickness is 10 nm. The hysteresis loops show counterclockwise traces and their shapes are almost the same regardless of the sweep rate. Generally, the $C-V$ hysteresis width of the metal-insulator-silicon (MIS) structure with mobile ions increases with decreasing sweep rate. In fact, we observed the sweep rate dependence of the hysteresis loop for the YSZ film deposited under strong plasma radiation. Decreasing the sweep rate increases bias duration to the YSZ film so that the drift distance of the mobile ions in the YSZ film increases and the difference in threshold voltage increases in the dual $C-V$

Fig. 10

curves. Therefore, we can say that the $C-V$ hysteresis loop in Fig.10 is not derived mainly from ion drift. At present, however, we do not know whether this hysteresis loop arises from ferroelectric polarization or from charge injection into the m-PZT film from the top electrode. If charge is injected into the m-PZT film, it may be trapped in the film and at the interface. Further, if the trapped charge induces charge in Si and detrapping of this trapped charge does not follow with the variation of the applied voltage, a counterclockwise hysteresis loop may occur. According to the cross-sectional TEM image of the sample of Fig.10, an about 4.5-nm-thick silicon oxide layer was formed between the 10-nm-thick YSZ layer and the Si substrate. Assuming that the relative dielectric constant of the YSZ layer is 27[17,28] and that the transition layer is silicon dioxide (SiO_2) with a relative dielectric constant of 3.9, the accumulation capacitance of the YSZ/SiO_2/Si structure per unit area is calculated to be about 580 nF/cm^2. Since this calculated accumulation capacitance is almost equal to the experimental one of about 530 nF/cm^2 (Fig.9), this assumption is valid in our case and we can say that the YSZ/SiO_x layer capacitance was hardly changed by depositing the m-PZT film. Using the calculated and experimental YSZ/SiO_2 capacitances of 580 and 530 nF/cm^2, respectively, the relative dielectric constants of the m-PZT film are estimated to be 43 and 46, respectively, from the accumulation region capacitance of 230 nF/cm^2 in Fig.10. These values are much smaller than the reported values of the perovskite PZT film. In this calculation, we assumed that the dielectric constant of the pyrochlore interfacial layer was equal to that of the m-PZT film because the accumulation capacitance of the 100-nm pyrochlore/10-nm YSZ/Si structure was almost the same as that in Fig.10.

4. Discussion

First, we discuss the crystal structure of the m-PZT film and make a rough estimation of its lattice parameters. Based on the TEM images and the SAD patterns in Fig.6, we assume that the crystal structure of the PZT film grown at $T_S \leq 470°C$ is monoclinic with $\alpha=\beta=90°$ as shown in Fig.11. According to this assumption, in the $2\theta-\theta$ diffraction pattern of the PZT film grown at 460°C, the peaks at 2θ=30.97, 107.2, 36.22 and 77.17° are regarded as the reflections from (110), (330), $(\bar{1}10)$ and $(\bar{2}20)$, respectively. The reflection angle of m-PZT(220) overlaps with the tail of the Si(400) peak so that it is not used. These angles depend on the lattice constants $a=b$ and the lattice angle γ. Also, the peak at $2\theta=79.38°$ in the ϕ scan measurement is regarded as the reflection from (131) and this angle depends on all the lattice parameters. Using these measurement values, calculation gives 0.379 nm for $a=b$, 0.521 nm for c and 81.3° for the lattice angle γ. In this calculation, the plane distances d of (110) and $(\bar{1}10)$ were obtained from the intercept of the line extrapolated to the d axis in the plots of d vs $cos^2\theta/sin\theta$ in order to reduce measurement error.[29] By using these calculated lattice parameters, the plane distances of (120) and (230) are estimated to

Fig. 11

be 0.176 and 0.111 nm, respectively. They are roughly equal to the experimental values of 0.179 and 0.112 nm obtained from ϕ scan measurement. Also, these lattice parameters almost coincide with those estimated from the SAD patterns within a 1% error. Based on these lattice parameters, the schematic SAD patterns of Figs.6(c) and 6(d) are shown in Figs.12(a) and 12(b), respectively, with the deflection indices. The deflection indices can be labeled without contradiction. Hence, it can be said that these lattice parameters and the assumed monoclinic crystal structure are valid in our experimental results. Recently, Noheda *et al.* discovered a new monoclinic ferroelectric phase in the $Pb(Zr_{0.52}Ti_{0.48})O_3$ solid solution and reported that the lattice parameters are a_m = 0.5717 nm, b_m = 0.5703 nm, c_m = 0.4143 nm and β = 90.53° at 20 K.[30] This new phase appears below 210 K and is transformed into the normal perovskite phase at the room temperature. This phase transformation is very different from our case in which the m-PZT phase appears at the room temperature but is changed to the pyrochlore phase irreversibly by annealing at temperatures above 350°C. Also, the TEM images and SAD patterns in Fig.6 can not be explained by the lattice parameters assigned to Noheda *et al.*'s monoclinic PZT phase. Therefore, our m-PZT film is an unreported phase as far as we know. Further, the epitaxial temperature of the m-PZT film of 435°C is lower than many of those reported for epitaxial perovskite PZT films.[6,7,31–33] The unit size of m-PZT(110) is about 0.494×0.521 nm^2 and is nearly equal to that of YSZ(100)(0.514×0.514 nm^2) as shown in Fig.11. This small lattice mismatch of 1.4 to 3.9% suggests that the crystal information of the YSZ buffer layer strongly influences the crystal growth of the m-PZT film. Also, the epitaxial double domain of the m-PZT film is a mixture of m-PZT[$\bar{1}$10]//YSZ[010] and m-PZT[001]//YSZ[010]. This means that the heteroepitaxial m-(110) PZT film on the (100) YSZ layer is formed by the competitive growth of single m-(110) PZT domains because the crystallographic relationship of m-PZT[$\bar{1}$10]//YSZ[010] is equivalent to that of m-PZT[001]//YSZ[010] on cubic (100) YSZ.

Fig. 12

Next, we will discuss the low resistivity of the as-grown m-PZT film. Using a Nomarski optical microscope, we observed that the surface of the m-PZT film was fairly smooth. Although the step-annealing process degrades crystalline quality slightly as shown in Figs.4(b) and 5, the leakage current of the annealed sample is further reduced. Therefore, we can say that surface roughness and crystalline defects are not responsible for the low resistivity of the m-PZT film. From the result in Fig.3, it is inferred that the high content of oxygen is related to the low resistivity of the m-PZT film. ZrO_2 and TiO_2 are much stabler than PbO because the free energies of formation of ZrO_2 and TiO_2 are much lower than that of PbO.[34] Also, there are some reports that the PZT film contains lead oxide with an oxygen-rich phase, *e.g.*, $PbO_{1.44}$, Pb_2O_3, Pb_3O_4 and PbO_2, under growth or annealing temperature lower than 700°C.[35–37] The Pb oxidation state of Pb^{2+} is stabler than that of Pb^{4+}, and PbO_x except PbO and PbO_2 is a mixed valence

compound of Pb^{2+} and Pb^{4+}. Therefore, it is possible that most of the excess oxygen in the as-grown m-PZT film form a chemical bond with Pb. In the case of Fe_3O_4 which exhibits the same linear relationship between $\log(I)$ and T as shown in Fig.8,[24,25] electron tunneling occurs between degenerate levels on adjacent ions such as $Fe^{2+} \rightarrow Fe^{3+}$. Hence, for the case of as-grown m-PZT, it is possible that electron tunneling between Pb^{2+} and Pb^{4+} leads to the relatively low resistivity as shown in Figs.7 and 8.

On the other hand, the resistivity of the m-PZT film is increased by step- annealing as shown in Fig.7. We obtained the following experimental results from the step-annealed samples. (1) From RBS and XRD measurements, it was found that the chemical composition and the crystal structure of the m-PZT film were hardly changed by the step-annealing process. (2) The etching time of the as-grown 100-nm-thick m-PZT film with 1% HF solution required more than one hour, which was much longer than that of the perovskite PZT film prepared at 650°C, *i.e.*, less than 15 s. However, the etching time of the step-annealed m-PZT film was much shorter, 30 to 120 s. The second experimental result implies that the chemical bonding state of the m-PZT film, in particular, the Pb-O bonding state, was changed by the step-annealing process because the etching rate depends on the state of the chemical bonds or the oxidation state. Since the Pb^{4+} state is more unstable than the Pb^{2+} state so that PbO_2 dissolves into $PbO_x (x < 2)$ at temperatures $> 300°C$,[38] we speculate that the 4+ state in theas-grown m-PZT film was gradually changed to the 2+ state by the step-annealing process. As a result, electron tunneling between the 4+ and 2+ states is reduced and the resistivity of the m-PZT film is increased. According to the experimental result (1), we consider that excess oxygen whose bond with Pb^{4+} has been broken by the step-annealing process remains in the sample and keeps the monoclinic crystal structure. As the lattice constant c of m-PZT is much larger than that of normal perovskite PZT, the excess oxygen maybe occupy an interstitial site in the crystal to expand the lattice. This speculation is supported by the following experimental results. RBS measurement of the phase-transformed and pyrochlore PZT film in Fig.4(a) showed that the oxygen ratio was decreased to 2.9-3.0 and that other chemical composition ratios were almost the same as those of the as-grown film. Furthermore, the thickness of the phase-transformed PZT film was found to be decreased by about 10% compared with the as-grown one, which means that the density of the pyrochlore phase is higher than that of m-PZT phase. These results can be explained by the release of excess oxygen from the as-grown film during phase transformation. After the release of excess oxygen, the m-PZT film hardly retains its crystal structure due to elastic strain so that it deforms into the stabler pyrochlore structure.

We still have one question, that is, why the m-PZT phase is transformed into the pyrochlore phase as shown in Fig.4(a) by the annealing process whose temperature is lower than the temperature for deposition. In other words, why can the m-PZT film retain its phase during

deposition at a higher substrate temperature than that of the annealing process? We found that the phase transformation occurred upon annealing in N_2 atmosphere at 400°C for 30 min but not upon annealing at a pressure of about 3×10^{-5} Pa at 485°C for 30 min. Thus, it can be inferred that regardless of the kind of gas, a higher gas pressure may play the role of assisting the transformation from the low density m-PZT phase to the high density pyrochlore phase. Also, it is known that PbO_2 can be produced from PbO by a photochemical reaction in O_2 gas atmosphere.[39] Therefore, we can speculate that the optical irradiation from the plasma and low Ar+O_2 gas pressure during sputtering deposition retain the monoclinic phase of the PZT film even at temperatures higher than 400°C. Also, the phase transformation may occur easily under the annealing conditions of high pressure and little optical irradiation except infrared from the annealing furnace.

5. Conclusions

We investigated the crystalline and electrical properties of epitaxial PZT films grown on Si covered with epitaxial (100) YSZ buffer layers. PZT films were prepared by reactive sputtering at substrate temperature $T_S \leq 520$°C. When the substrate temperature was between 400 and 485°C, we obtained a heteroepitaxial (110)-oriented monoclinic PZT film that did not have the normal perovskite phase. The lattice parameters were as follows: $a = b = 0.379$ nm, $c = 0.521$ nm and $\gamma = 81.3°$. The lattice mismatch was small, *i.e.*, less than 4%, between the unit area of m- PZT (110) and YSZ (100). Thus, it is possible that the lattice of the epitaxial (100) YSZ layer induced the formation of this new PZT phase. However, the pyrochlore phase grew at $T_S \geq 495$°C and the m-PZT film was transformed into the pyrochlore phase by the normal conventional annealing process at temperatures higher than 350°C. Therefore, the m-PZT phase is considered to be metastable and has the following features. The as-grown film has a larger oxygen composition ratio O/(Zr+Ti) of 3 .2 to 3.8 than the pyrochlore and perovskite phases. Although the resistivity of the as-grown m- PZT film is much lower than that of the normal perovskite phase, it is increased by two to five orders of magnitude by the step-annealing process without changing the chemical composition and the crystal structure. This resistivity behavior can be explained by the chemical bond between excess oxygen and Pb. In the as-grown film, electron tunneling between the Pb oxidation states of 4+ and 2+ occurs, but in the post-annealed film, the 4+ state is changed to the 2+ state so that electron conduction is reduced. The $C-V$ characteristics of thestep-annealed m-PZT/YSZ/Si structure showed counterclockwisehysteresis loops. These loops are probably due to the ferroelectricity of the m-PZT film or the charge injection into the m-PZT film from the top electrode. To clarify this point, further investigation is necessary. Since the m-PZT film has a low relative dielectric constant of about 45 and can be prepared at low deposition temperatures, it is supposed to be a good candidate for the gate material of MFIS-FET.

Acknowledgements

We thank Mr. K.Yamamoto of Kobelco Research Institute Inc. for TEM observation and useful comments. This work was partially supported by the Murata Science Foundation.

References

1) J.L.Moll and Y.Tarui: IEEE Trans.Electron Devices **10**(1963) 338.
2) T.Hirai, K.Teramoto, K.Nagashima, H.Koike and Y.Tarui: Jpn.J.Appl.Phys. **34**(1995)4163.
3) Y.Shichi, S.Tanimoto, T.Goto, K.Kuroiwa and Y.Tarui: Jpn.J.Appl.Phys. **33**(1994)5172.
4) A.Masuda, Y.Yamanaka, M.Tazoe, Y.Yonezawa, A.Morimoto and T.Shimizu: Jpn.J.Appl.Phys. **34**(1995)5154.
5) J.Senzaki, K.Kurihara, N.Nomura, O.Mistunaga, Y.Iwasaki, and T.Ueno: Jpn.J.Appl.Phys. **37**(1998)5150.
6) E.Tokumitsu, K.Itani, B.-K.Moon and H.Ishiwara: Jpn.J. Appl.Phys. **34**(1995)5202.
7) T.Hirai, K.Nagashima, H.Koike, S.Matsuno and Y.Tarui: Jpn.J.Appl.Phys. **35**(1996)5150.
8) B.-E.Park, S.Shouriki, E.Tokumitsu and H.Ishiwara: Jpn.J. Appl.Phys. **37**(1998)5145.
9) T.Maruyama, M.Saitoh, I.Sakai, T.Hidaka, Y.Yano and T.Noguchi: Appl.Phys.Lett. **73**(1998)3524.
10) M.de Keijser, J.F.M.Cillessen, R.B.F.Janssen, A.E.M.De Veirman and D.M.de Leeuw: J.Appl.Phys. **79**(1996)393.
11) C.M.Foster, G.-R.Bai, R.Csencsits, J.Vetrone, R.Jammy, L.A.Wills, E.Carr and J.Amano: J.Appl.Phys. **81**(1997)2349.
12) S.Horita, T.Kawada and Y.Abe: Jpn.J.Appl.Phys. **35**(1996) L1357.
13) S.Horita, T.Naruse, M.Watanabe, A.Masuda, T.Kawada and Y.Abe: Appl.Surf.Sci. **117/118**(1997)429.
14) P.Legagneux, G.Garry, D.Dieumegard, C.Schwebel, C.Pellet, G.Gautherin and J.Siejka: Appl.Phys.Lett. **53**(1988)1506.
15) T.Hirai, K.Teramoto, K.Nagashima, H.Koike, S.Matsuno, S.Tanimoto and Y.Tarui: Jpn.J.Appl.Phys. **35**(1996)4016.
16) S.Yamauchi, H.Tamura, M.Yoshimaru and M.Ino: Jpn.J. Appl.Phys. **32**(1993)4118.
17) S.Yamauchi and M.Yoshimaru: Jpn.J.Appl.Phys. **35**(1996) 1553.
18) S.Horita, M.Murakawa and T.Fujiyama: Jpn.J.Appl.Phys. **34**(1995)1942.
19) J.-D.Kim, S.Kawagoe, K.Sasaki and T.Hata: Jpn.J.Appl.Phys. **38**(1999)6882.
20) Th.Matthée, J.Wecker, H.Behner, G.Friedl, O.Eibl and K.Samwer: Appl.Phys.Lett. **61**(1995)1240.
21) T.Inoue, T.Ohsuna, Y.Yamada, K.Wakamatsu, Y.Itoh, T.Nozawa, E.Sasaki, Y.Yamamoto and Y.Sakurai: Jpn.J. Appl.Phys. **31**(1992)L1736.
22) S.-T.Kim, H.-H.Kim, Y.-I.Kim, M.-Y.Lee and W.-J.Lee: Jpn.J.Appl.Phys. **36**(1997)5663.
23) S.Fujii, I.Kanno, T.Kamada and R.Takayama: Jpn.J. Appl.Phys. **36**(1997)6065.
24) W.R.McKinnon, C.M.Hurd and I.Shiozaki: J.Phys.C **14**(1981)L877.
25) M.Pai and J.M.Honig: J.Phys.C **16**(1983)L35.
26) D.B.Fenner, A.M.Viano, D.K.Fork, G.A.N.Connell, J.B.Boyce, F.A.Ponce and J.C.Tramontana: J.Appl.Phys. **69**(1991)2176.
27) S.Horita, M.Watanabe, S.Umemoto and A.Masuda: Vacuum **51**(1998)609.
28) M.T.Lanagan, J.K.Yamamoto, A.Bhalla and S.G.Sankar: Mater.Lett. **7**(1989)437.
29) B.D.Cullity: *Elements of X-Ray Diffraction* (Addison-Wesley, London, 1978) 2nd ed., p.359.
30) B.Noheda, D.E.Cox, G.Shirane, J.A.Gonzalo, L.E.Cross and S-E.Park: Appl.Phys.Lett. **74**(1999)2059.
31) Y.-M.Kim, W.-J.Lee and H.-G.Kim: Thin Solid Films **279**(1996)140.
32) W.Zhang, K.Sasaki and T.Hata: Jpn.J.Appl.Phys. **35**(1996) 5084.
33) J.-S.Shin, K.-S.No and W.-J.Lee: Jpn.J.Appl.Phys. **36**(1997) L223.
34) J.F.M.Cillessen, M.W.J.Prins and R.M.Wolf: J.Appl.Phys. **81**(1997)2777.
35) C.V.R.V.Kumar, R.Pascual and M.Sayer: J.Appl.Phys. **71**(1992)864.

36) V.Chikarmane, C.Sudhama, J.Kim, J.Lee, A.Tasch and S.Novak: J.Vac.Sci. & Technol.A **10**(1992)1562.
37) J.Schäfer, W.Sigmund, S.Roy and F.Aldinger: J.Mater.Res. **12**(1997)2518.
38) A.P.Thompson: *Encyclopedia of Chemical Technology*, eds. R.E.Kirk and D.F.Othmer (The Interscience Encyclopedia, New York, 1952) Vol.8, p.272.
39) K.Saito: *Kagaku Daiziten* (Kyoritsu Shuppan, Tokyo, 1993) Vol.3, p.928 [in Japanese].

Figure captions

Fig. 1. Substrate temperature dependence of XRD patterns of PZT films on Si covered with YSZ buffer layers. Thicknesses of the YSZ layers are 10 nm at $T_S = 460$ and $470°$C, and 100 nm at $T_S = 435$ and $495°$C. Thicknesses of the PZT films are 100 nm at $T_S = 460$ and $470°$C, and 200 nm at $T_S = 435$ and $495°$C. Reflection indices of the peak around 31and 36.2° are labeled, based on a monoclinic structure which is mentioned in §4. indicates the peak due to kβ m-PZT(110).

Fig. 2. ϕ scan patterns of m-PZT film grown at $T_S = 435°$C in Fig.1. Reflection indices are labeled, based on a monoclinic structure which is mentioned in §4.

Fig. 3. Dependence of composition ratio of as-grown PZT film on substrate temperature. Composition was estimated by RBS measurement. It is noted that the O/(Zr+Ti) ratio in region II is much larger than those in other regions.

Fig. 4. Typical XRD patterns of samples with m-PZT films prepared at (a) $T_S = 435$ and (b) $460°$C, where the samples had the 100-nm-thick m-PZT/10-nm-thick YSZ/Si structure. Sample (a) was annealed at 300°C for 30 min + 400°C for 30 min and sample (b) was step-annealed at 300°C for 120 min + 325°C for 120 min + 350°C for 180 min.

Fig. 5. RBS spectra of samples with (a) as-grown and (b) step-annealed 100-nm-thick PZT films on 10-nm YSZ/(100)Si substrates.

Fig. 6. Cross-sectional TEM images[(a) and (b)] and SAD patterns [(c),(d) and (e)]of the step-annealed m-PZT film, where the PZT film was grown at $T_S = 460°$C. The upper direction is toward the surface of the PZT film and the electron beam direction is Si $< 100 >$. Areas with numbers (1) to (4) show typical crystal structures.

Fig. 7. Leakage current density-voltage characteristics of as-grown and step-annealed samples with PZT film prepared at $T_S = 460°$C.

Fig. 8. Temperature dependence of electrical current I (A) at 3 V of as-grown m-PZT film deposited at $T_S = 460°$C. Data are plotted as log(I) versus T(closed circles) and $1/T$(open circles).

Fig. 9. $C - V$ characteristics of 10-nm-thick YSZ/Si substrate structure where sweep rate is 0.1 V/s and measurement frequency is 1 MHz.

Fig. 10. $C - V$ characteristics of step-annealed sample shown in Fig.4, where sweep rates are 0.1, 0.5 and 1.0 V/s. The hysteresis width is almost independent of the sweep rate.

Fig. 11. Schematic drawing of the m-PZT unit structure with the unit YSZ lattice plane.

Fig. 12. Schematic SAD patterns (a) and (b) of Figs.6(c) and 6(d), respectively, with deflection indices. (a) is for m-PZT $[1\bar{1}0]$ and (b) is for m-PZT [001]. The crystal structure is monoclinic as shown in Fig.11.

00R01054

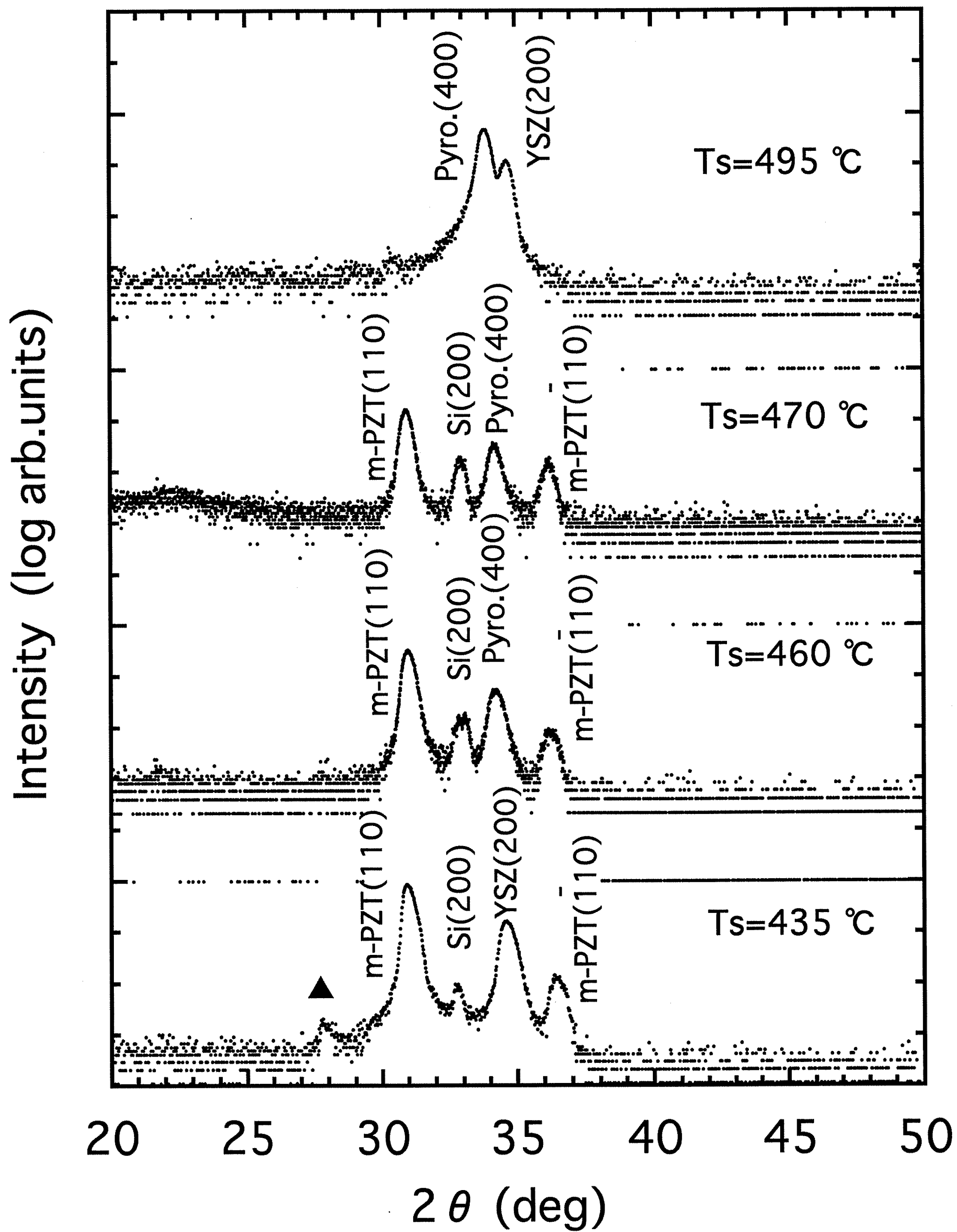

17 cm

Fig.1

S. Horita et al.
JJAP

080...

00R01054

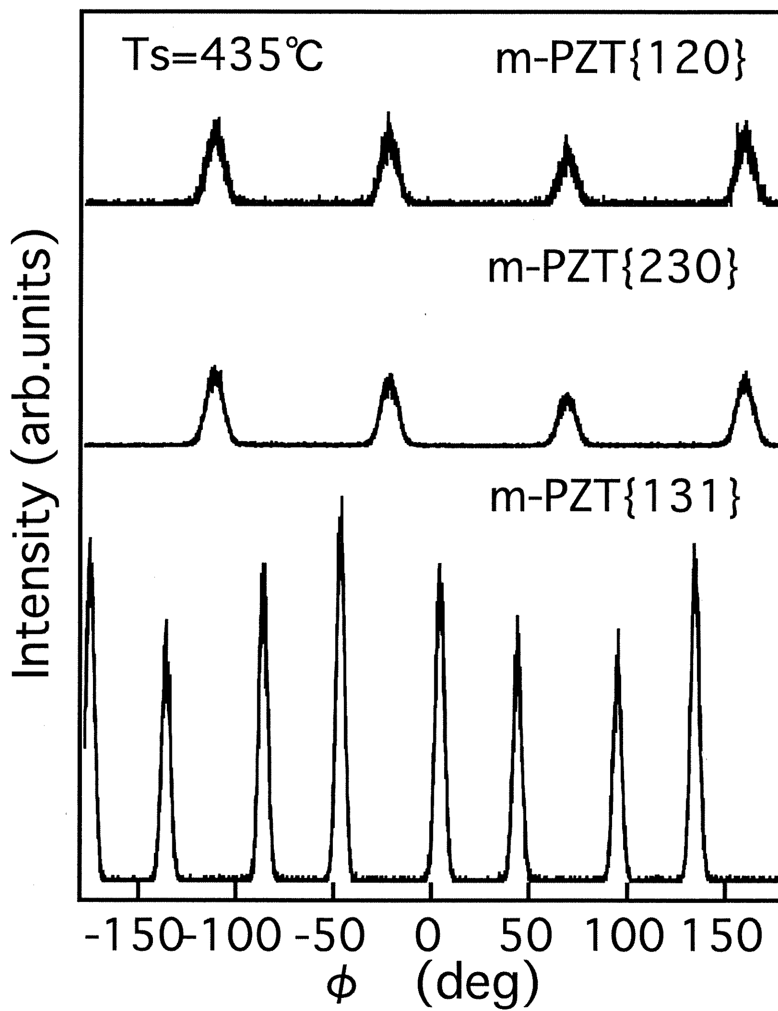

7 cm

Fig. 2

26

S. Horita et al
J.J.A.P.

080

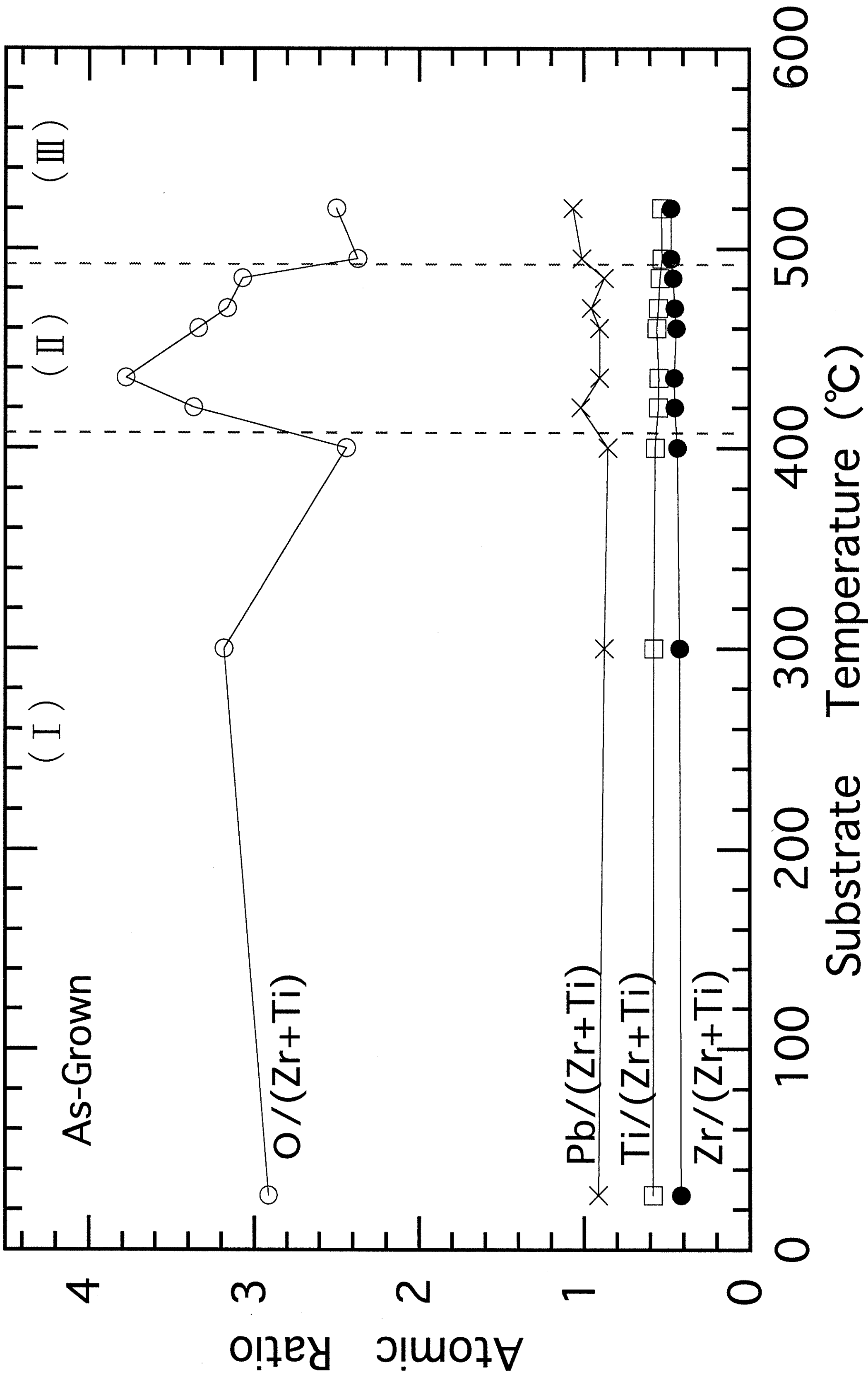

8.6cm

S.Horita et al

J.J.A.P.

Fig.3

080

00R01054

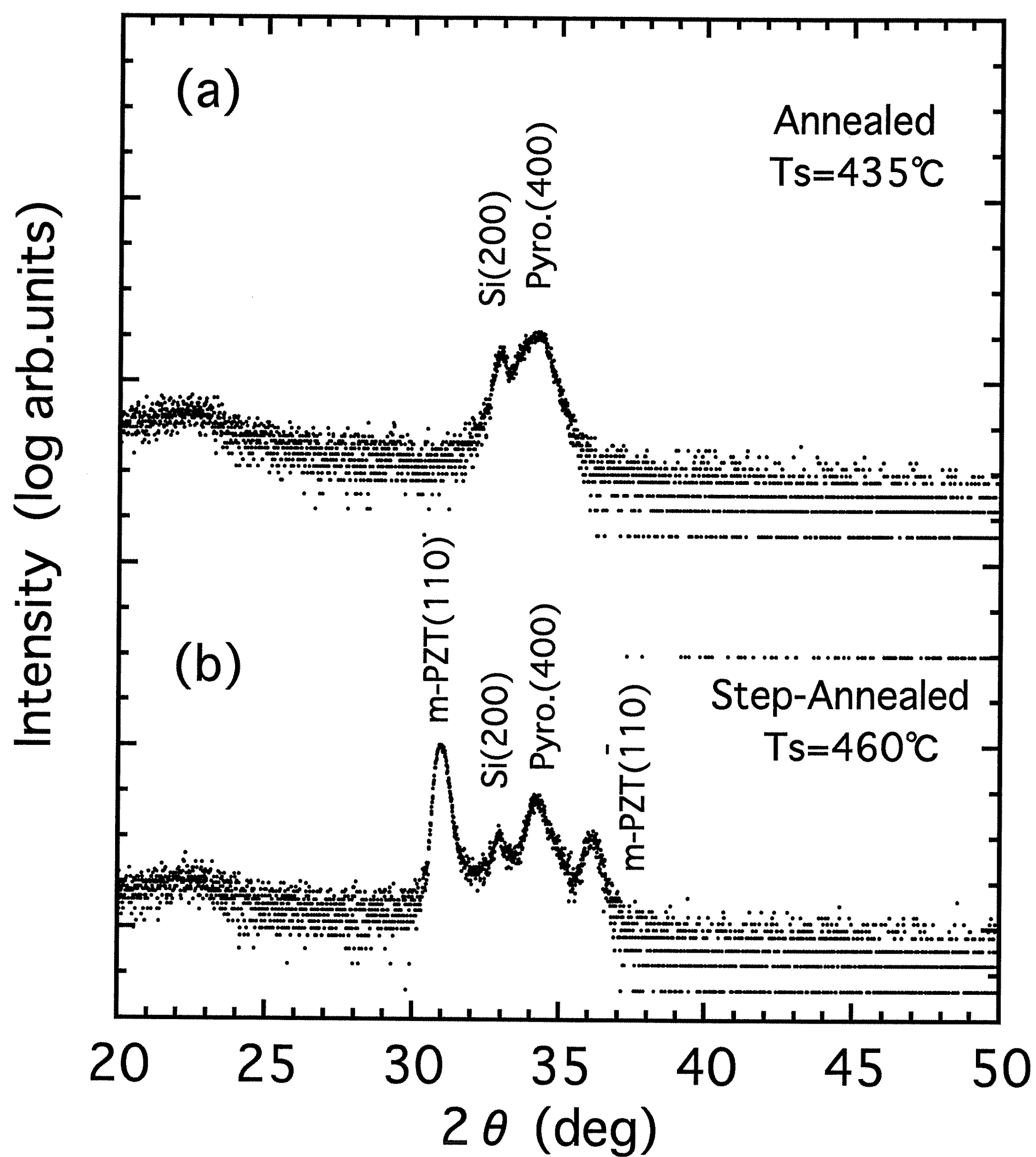

7 cm

S. Horita et al
J.J.A.P

Fig. 4

080350

00R01054

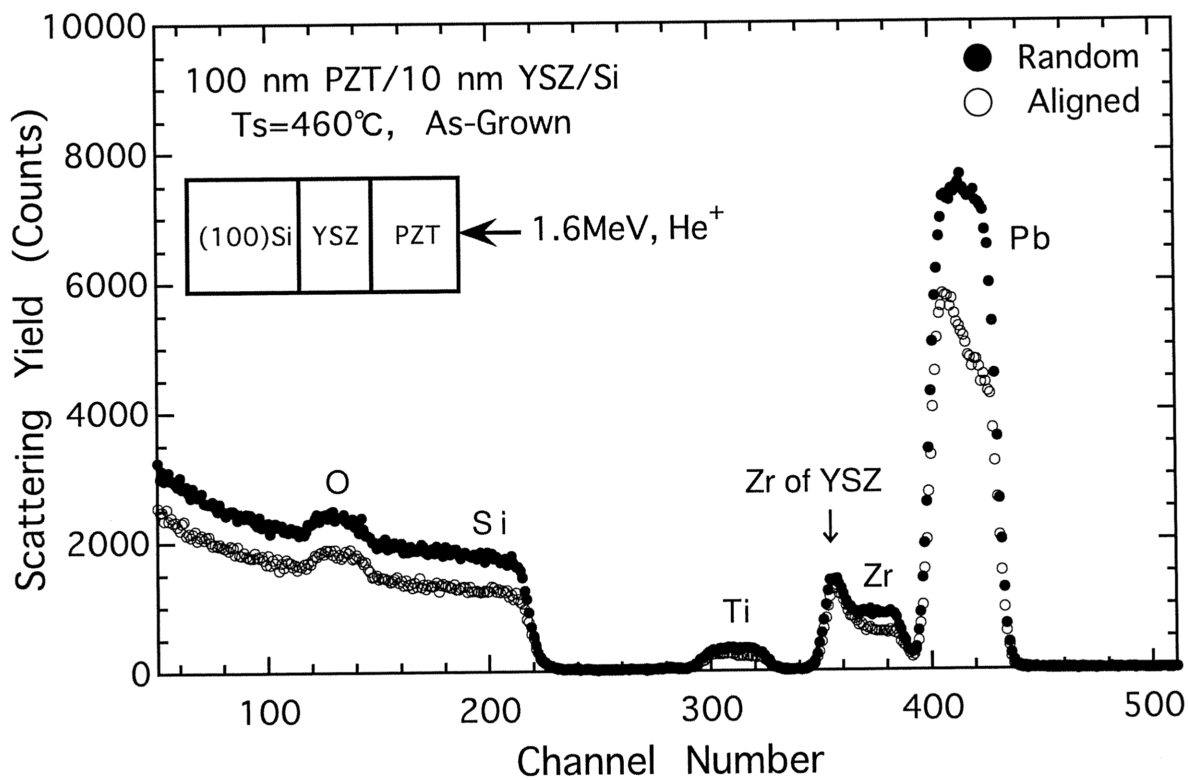

8.6cm

Fig.5(a)

080301

S. Horita et al.
JJAP

00R01054

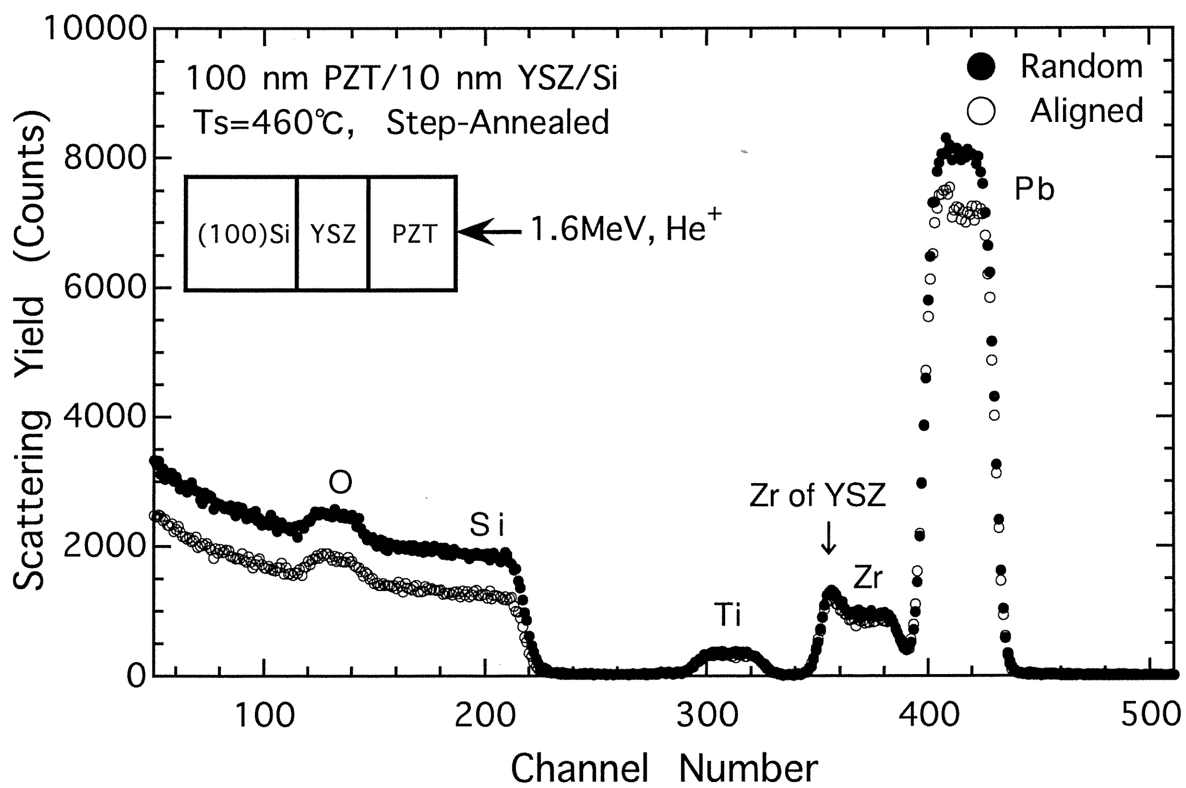

Fig.5(b)

8.6 cm

S. Horita et al,
JJAP

080352

00R01054

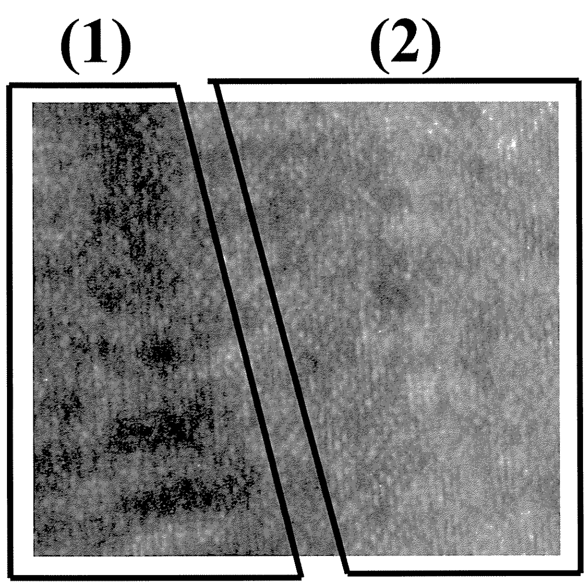

(a)

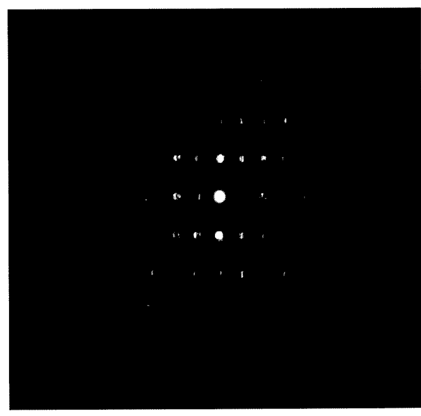

(c)

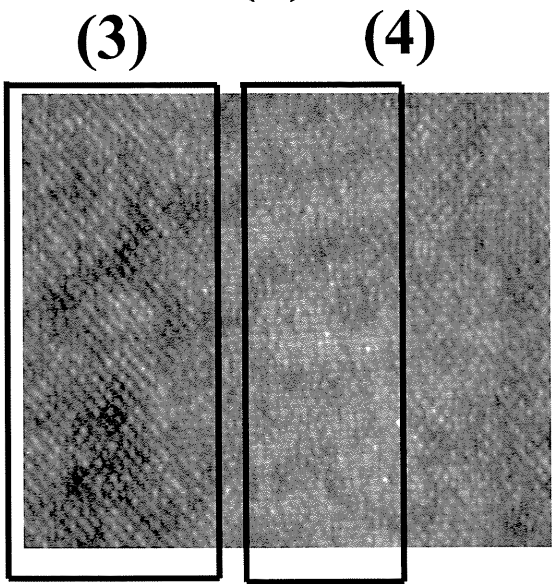

(b)

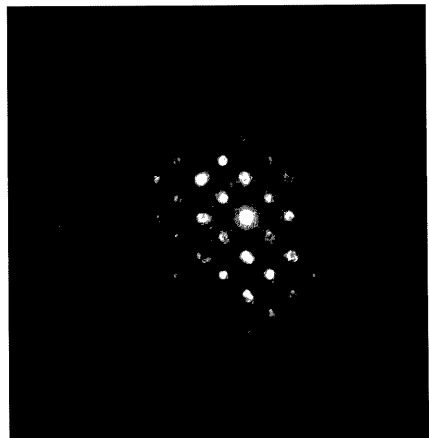

(d)

5 nm

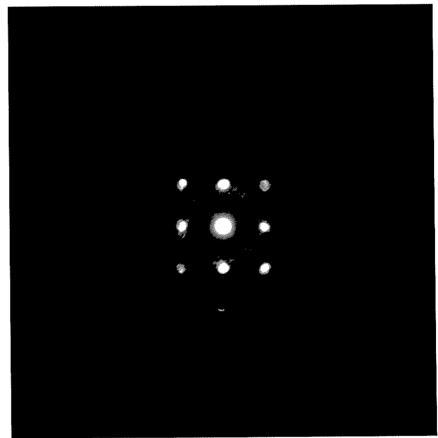

(e)

15 cm

Fig. 6

S. Horita et al.
J. J. A. P.

00R01054

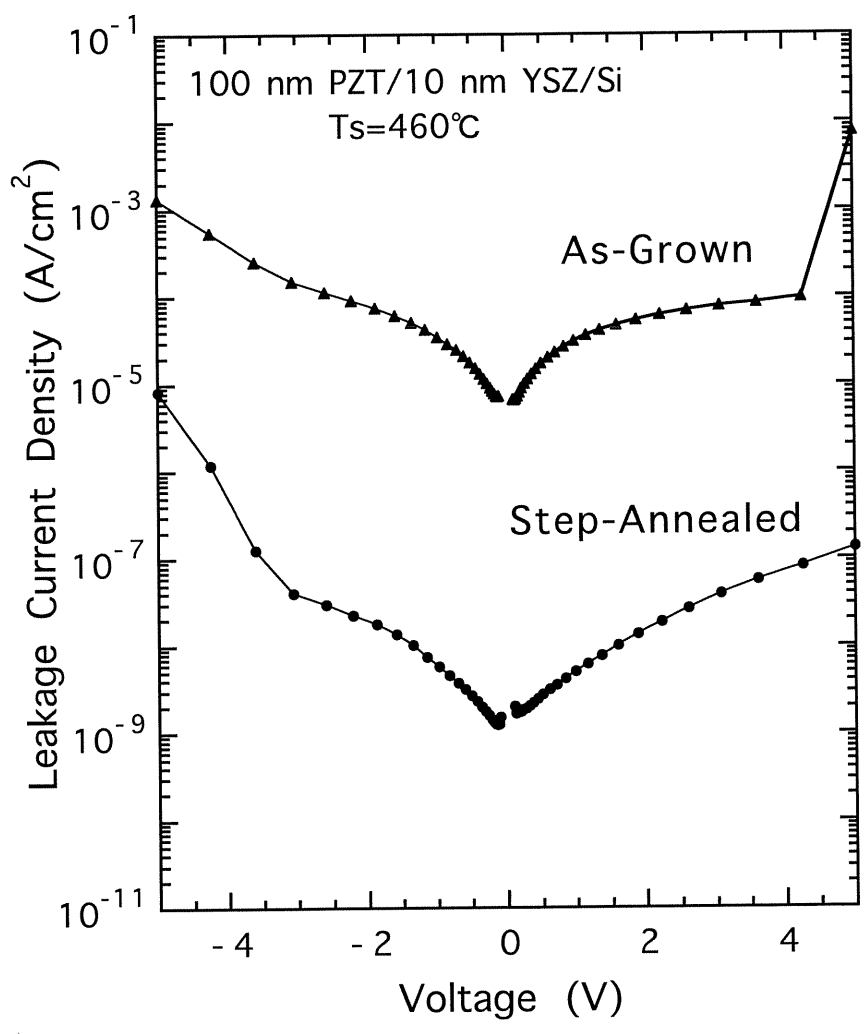

Fig.7.

7 cm
S. Morita et al
J.J.A.P

08028

00R01054

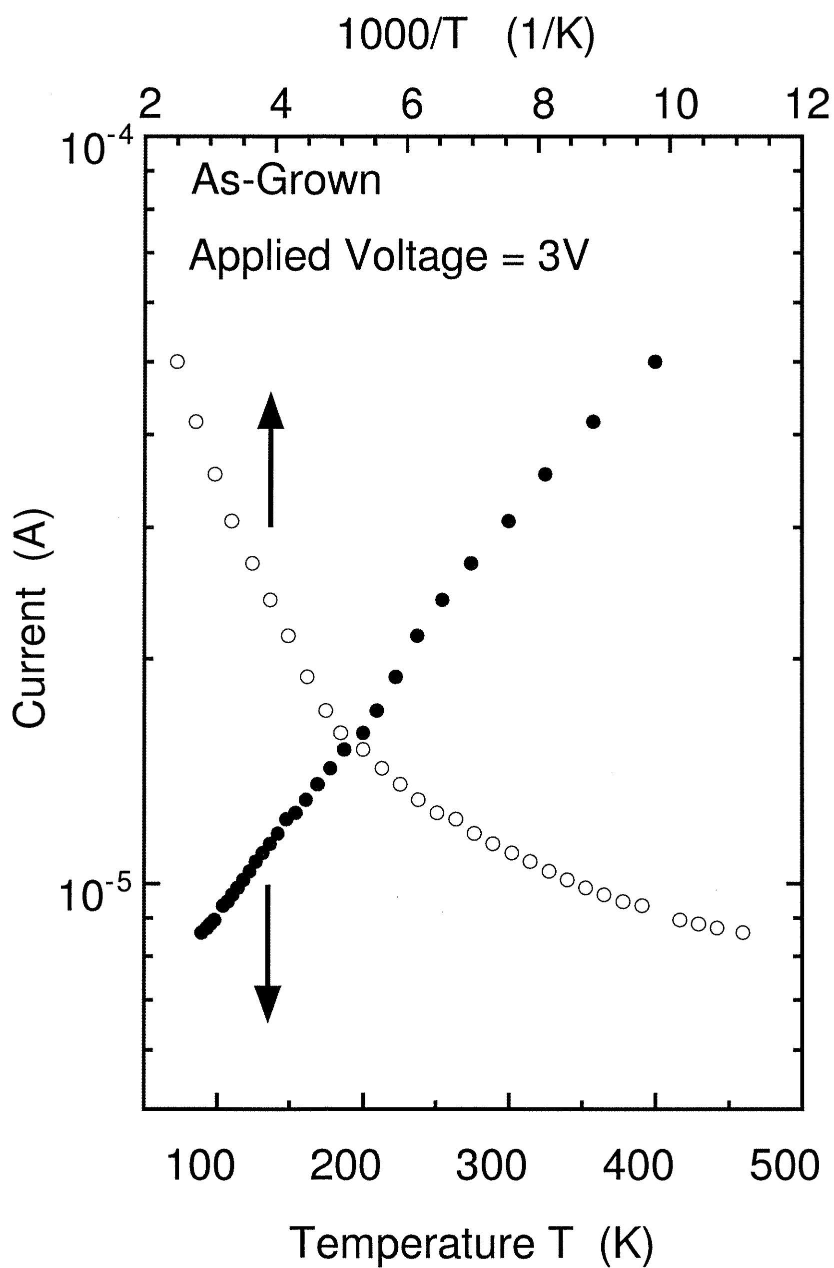

Fig.8

6cm
S.Horita et al
J.J.A.P.

080235

00R01054

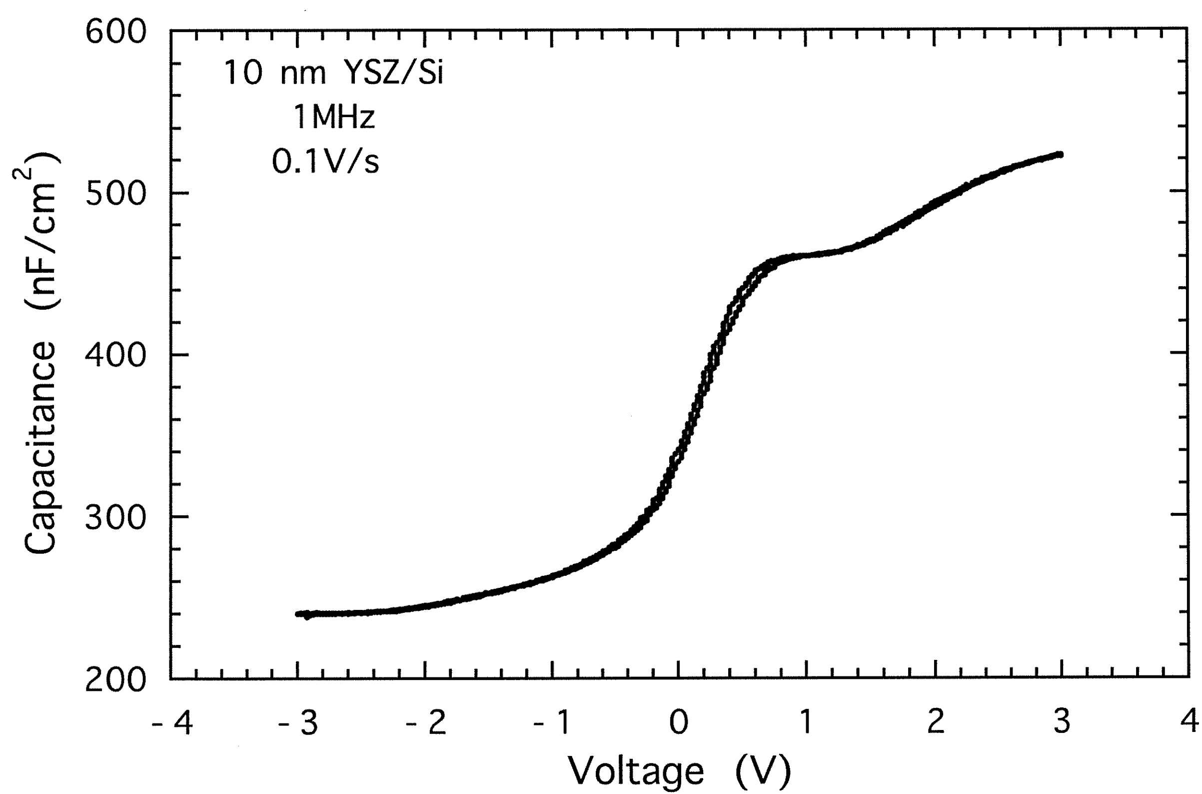

Fig.9

7 cm
S. Horita et al.
JJAP

080...

00R01054

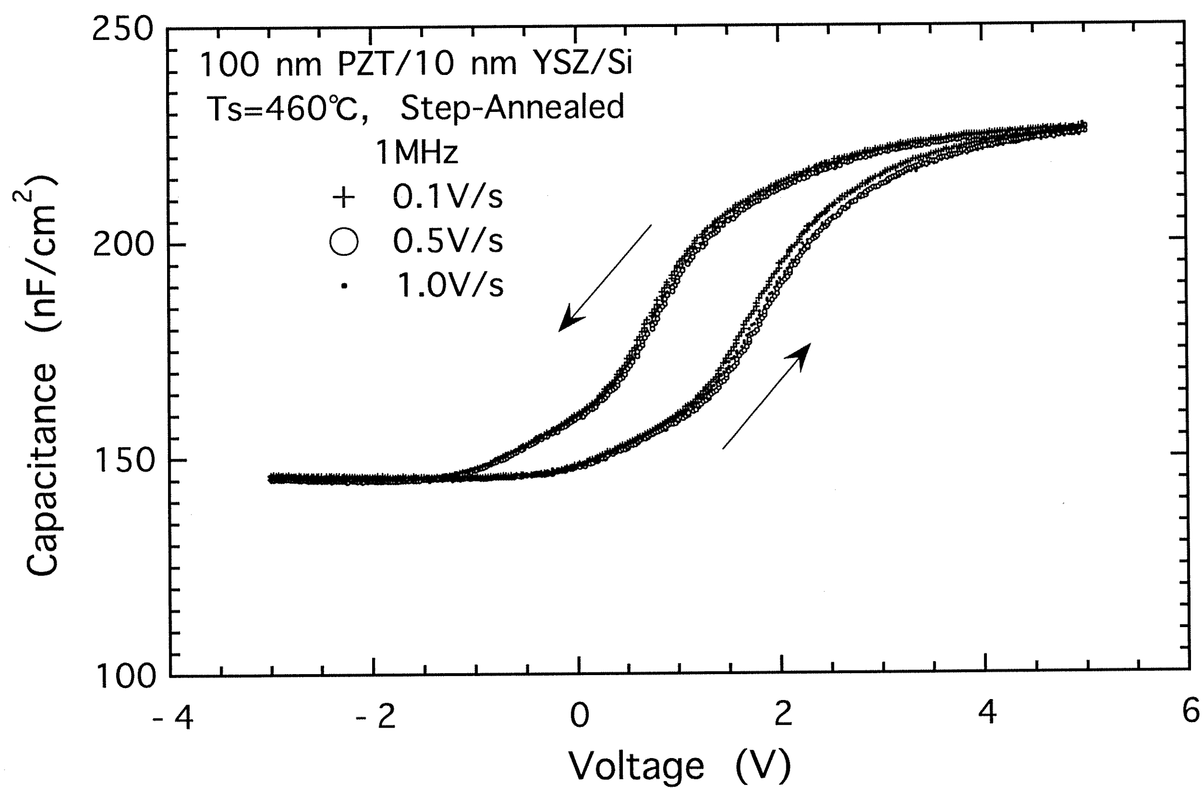

Fig.10

080237

7cm
S.Horita et al.
JJAP

00R01054

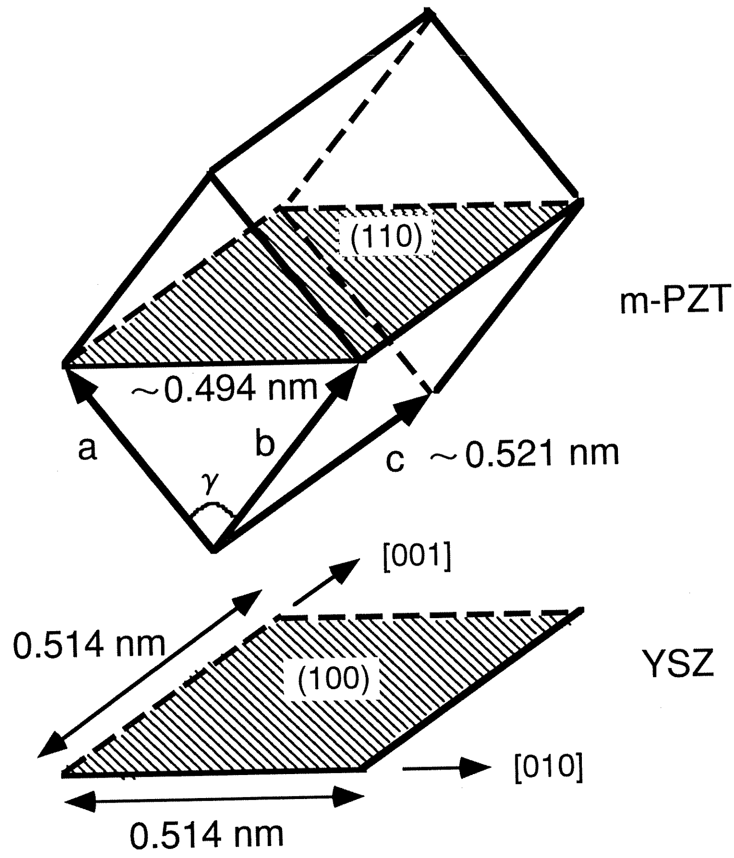

7 cm

S. Horita et al.

Fig. 11

080

J. J. A. P.

00R01054

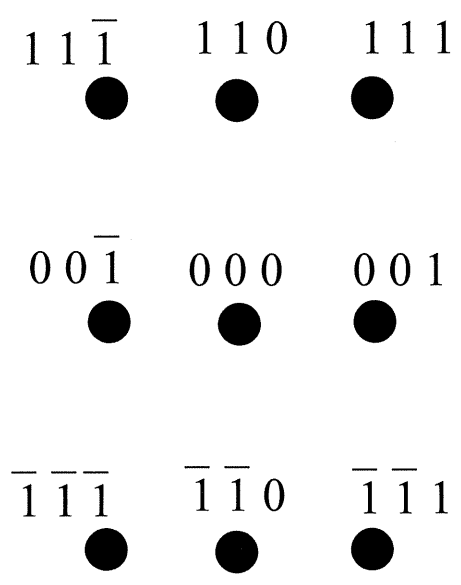

(a) m-PZT [1$\bar{1}$0]

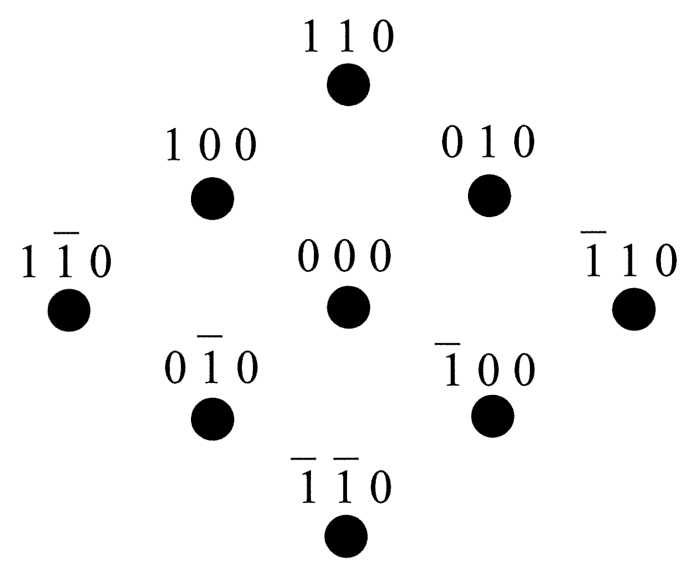

(b) m-PZT [001]

7cm

Fig. 12

S. Horita et al
J.J.A.P.